Correction Technique for Quality Improvement of Doublet Lattice Unsteady Loads by Introducing CFD Small Disturbance Aerodynamics

(Received: March 3, 2017. Revised: December 7, 2017. Accepted: December 24, 2017)

LUKAS KATZENMEIER[1]
CYRILLE VIDY[1]
CHRISTIAN BREITSAMTER[2]

Abstract
For aeroelastic analyses in the industrial context, the Doublet Lattice Method (DLM) is a widely used method since it provides conservative results with low computational effort. However, the DLM lacks in predicting discontinuous transonic phenomena (shock positions and intensity) and effects of complex three-dimensional geometries. Several other authors have established the need for an improvement of the DLM results with CFD or experimental data while preserving its advantage of low computational costs. The introduction of small-disturbance CFD aerodynamics into the aeroelastic analysis process led the way to combine an enhanced accuracy of the aerodynamics combined with a moderate computational effort. However, linearized CFD methods are still unhandy to use in the development process of a configuration since they are inflexible to design changes of the configuration. Therefore, the authors present a correction method to enhance the quality of DLM results by introducing few results from the small-disturbance CFD method *AER-SDEu* developed at the Institute of Aerodynamics at the Technical University of Munich. The method employs densely populated, diagonal dominant correction matrices to correct the downwash or the forces of the DLM based on an equality between the forces predicted by the corrected DLM and the CFD method. This leads to a significantly higher quality of the DLM results, even throughout potential design changes. The developed correction method is applied to two well-known configurations, namely the AGARD Wing 445.6 (weak. 3) and the Goland+ Wing.

Nomenclature

AIC	Matrix of aerodynamic influence coefficients
c_p	Pressure coefficient
c_r	Root chord
$\mathbf{f}$, $\mathbf{g}$, $\mathbf{h}$	Convective fluxes in cartesian coordiantes
$\mathbf{F}$, $\mathbf{G}$, $\mathbf{H}$	Convective fluxes in curvilinear coordiantes
$\mathbf{f}_{SD}$	Vector of disturbance forces from *AER-SDEu*
$\mathbf{F}_{SD}$	Matrix of disturbance forces from *AER-SDEu*
$\mathbf{G}$	Spline interpolation matrix
GAF	Matrix of generalized aerodynamic forces
$\mathbf{I}$	Unity matrix
k_{red}	Reduced frequency
Ma_∞	Free-stream Mach-number
p, p_∞	Pressure, free-stream pressure
$\mathbf{q}$	Vector of conservative variables in cartesian coordinates
$\mathbf{Q}$	Vector of conservative variables in curvilinear coordinates
$\mathbf{S}$	Diagonal matrix of box areas (DLM)
U_∞	Free-stream velocity
$\mathbf{w}$	Downwash vector

[1] Department of Structural Dynamics and Aeroelasticity, Airbus Defence and Space Manching, Germany
[2] Professor, Institute of Aerodynamics and Fluid Mechanics, Technical University of Munich Garching, Germany

doi:10.3293/asdj.2017.42

$\mathbf{W}$	Downwash matrix
$\mathbf{W}_a$, $\mathbf{W}_b$	Matrices with aerodynamic data from methods a and b
x, y, z	Cartesian coordinates
ξ, η, ζ	Curvilinear coordinates

Superscript

$\overline{()}$	Steady part
$\hat{()}$	1st order harmonic disturbed quantity

1. Introduction

Because of its robustness and low computational costs, the Doublet Lattice Method (DLM) [1] is a commonly used method for aeroelastic analyses (flutter and gust) of aircraft configurations for industrial applications. Especially during the development process of an aircraft, where the conceptual design undergoes substantial modifications, the advantages of the DLM regarding fast availability of the results and robustness of the modeling become relevant. However, the results of the DLM lack accuracy in predicting shock phenomena (intensity and position of shocks) and modeling complex three-dimensional structures (wing thickness and camber effects, complex fuselage structures, external stores, a.s.o.) [19]. Keeping in mind that such phenomena and configurational details can be crucial for the aeroelastic behavior of the aircraft, various nonlinear, unsteady CFD methods have been developed for conducting aeroelastic analyses including transonic flow effects and the full three dimensional aircraft configuration in the sense of a CFD method. Such fully unsteady CFD methods deliver results of high accuracy, but require excessive computational effort. Thus, linearized CFD methods (from Kreiselmaier and Laschka[15], Pechloff and Laschka [20] and Thormann and Widhalm [24]) have been developed to combine the advantages of computational savings of the DLM with the accuracy of CFD methods for aeroelastic application. As an example, the small disturbance Euler-method *AER-SDEu* has been applied to a wide range of simple to highly complex configurations for flutter and gust analyses (see Kreiselmaier and Laschka [15] , Fleischer and Breitsamter [6] and Vidy et al. [25]).

Although linearized CFD methods provide exceptional computational savings compared to fully unsteady CFD methods (up to ten times faster), they are unhandy to be used during the development process since they are inflexible to design changes of the aircraft configuration. The present paper therefore presents a method to correct modal DLM results for an aircraft configuration with modal small disturbance CFD results obtained from *AER-SDEu*. The correction is intended to enhance the quality of the DLM results in its common application range of the flight envelope (including limited transonic effects) while reducing the computational effort compared to purely CFD-based methods. Thereby, a densely populated, diagonal dominant correction matrix is used to correct the results obtained from DLM. A densely populated correction matrix is employed, since several other approaches have proven that a purely diagonal correction matrix prevents the method to correct the results qualitatively (e.g. [8], [13]). The robustness and applicability of the presented method is increased by the possibility to include several modes through a fully populated correction matrix. Correction matrices are computed for different values of reduced frequency k_{red} and Mach numbers Ma_∞. Thus, the correction matrices for other values of k_{red} and Ma_∞ can be obtained through interpolation.

The given paper first delivers a short outline of both, the DLM and *AER-SDEu* as a representative method for small disturbance CFD approaches. Afterwards, the general approach to the development of the correction factors is presented, followed by the detailed application to the aforementioned methods. Results for the AGARD Wing 445.6 (weak. 3) and the Goland+ Wing demonstrate the applicability of the developed correction method and its significant advantages w.r.t. computational savings and accuracy in the process of aircraft development.

2. Aerodynamic Methods

The following section gives a short overview over the aerodynamic methods used in the present paper. Although the developed correction technique can be applied to a range of aerodynamic methods, it is presented in a form to correct results from unsteady potential methods with results from linearized CFD methods. Since it is commonly used in industrial aeroelastic analyses, the Doublet Lattice Method from Albano and Rodden [1] is chosen as a representative method for linear unsteady potential methods. The linearized CFD method *AER-SDEu* from the Technical University of Munich is selected as a representative linearized CFD code, since it was used to gain a lot of experience analyzing configurations from airfoils to wings and full configurations [15, 6, 7, 25].

2.1 Doublet Lattice Method (DLM)

The DLM is a linear, unsteady potential method based on the Integral Equation of Unsteady Lifting Surface Theory and was introduced by Albano and Rodden [1]. Founded on unsteady potential theory, it describes an unsteady, inviscid and irrotational flow neglecting nonlinear effects. Hence, it does not consider shock effects, boundary layer separations, a.s.o. Furthermore, the method does not include the influence of three-dimensional geometries as thickness and camber effects or complex three dimensional structures.

The Integral Equation of Unsteady Lifting Surface Theory provides a relation between the induced unsteady downwash field $\hat{\mathbf{w}}$ and the unsteady pressure distribution $\Delta\hat{\mathbf{c}}_p$ of the configuration. Thereby, the lifting surface is modeled with several aerodynamic panels together assembling the whole lifting surface. The panels themselves consist of a finite number of boxes, where each box is a trapezoidal element with the parallel edges arranged in streamwise direction. The Integral Equation of the Lifting Surface Theory is solved on each box.

The downwash vector $\hat{\mathbf{w}}$ is known from the geometry of the configuration and the free flow velocity through the kinematic flow condition (cf. Blair [3]) applied to the 3/4-points of the configuration (the so called *Pistolesi-Point*). The method is based on the acceleration potential represented by doublets arranged on the quarter-line of each box. Assuming harmonic motion, the integral equation for each box reads (cf. Blair [3])

$$\hat{w}(x, y, z) = \frac{1}{8\pi} \iint\limits_A \Delta\hat{c}_p K(x, \xi; s, \sigma; \omega, Ma_\infty) \mathrm{d}\sigma \mathrm{d}\xi, \tag{1}$$

with the complex Kernel-function (cf. Blair [3])

$$\begin{aligned} K(x_0, y_0, z_0) = & \exp\left(\frac{-i\omega x_0}{U_\infty}\right) \\ & \cdot \frac{\partial^2}{\partial z^2}\left[\int\limits_{-\infty}^{x_0} \frac{1}{R} \exp\left[\frac{i\omega}{U_\infty \beta^2}(\lambda - Ma_\infty R)\right] \mathrm{d}\lambda\right]. \end{aligned} \tag{2}$$

The kinematic flow condition has to be satisfied at as many points as doublets are arranged. Thus, a system of equations develops with the number of equations equal to the number of boxes. The system of equations writes

$$\Delta\hat{\mathbf{c}}_p = \mathbf{AIC}\hat{\mathbf{w}} \tag{3}$$

with the matrix of aerodynamic influence coefficients **AIC**.

The generalized aerodynamic forces (GAFs) are then computed using

$$GAF_{ij} = \sum_{k=1}^{n} h_k^i \Delta\hat{c}_{p,k}^j \overline{S}_k. \tag{4}$$

with n being the number of boxes, h_k^i the deformation normal to the panel at the quarter point of box k for mode i, $\Delta\hat{c}_{p,k}^j$ the pressure difference coefficient on the quarter point of box k for mode j and $\overline{S}_k$ being the surface area of box k. Further details on the Doublet-Lattice-Method are given by Rodden [1].

2.2 Small Disturbance Euler Method (*AER-SDEu*)

The small-disturbance Euler-method *AER-SDEu* was developed at the Institute of Aerodynamics and Fluid Mechanics at the Technical University of Munich to combine the accuracy of a CFD method with the computational savings of linearized methods (cf. Kreiselmaier and Laschka [15]). The linearized CFD results in frequency domain can then be used in aeroelastic analyses, e.g. flutter analyses or gust response. A lot of experience has been gained with the method since it has been applied to configurations of various complexity (cf. Vidy et al. [25]).

Thereby, the method is based on a linearization of the Euler equations w.r.t. time around a steady, nonlinear reference state computed with the nonlinear method *AER-Eu*. Using this linearization, the method computes the disturbed aerodynamic quantities resulting for small and harmonic motion of the configuration in the frequency domain. The generalized aerodynamic forces (GAFs) are computed using the resulting disturbance pressures and the modal disturbance, i.e. the deflection. The advantage of the method compared to potential methods are a higher accuracy of the results in the transonic flow regime (shock phenomena) and the inclusion of geometric effects of the considered configuration, e.g. wing thickness and camber. The following section provides an overview over the linearization of the Euler equations and their numerical treatment in *AER-SDEu*.

The Euler equations describe a system of five coupled, nonlinear, partial differential equations of first order and hyperbolic character [10, 11]. They consist of the differential equations describing the conservation of mass, momentum and energy for an inviscid flow without thermal conduction. Since the airflow has six degrees of freedom, the system of equations is closed by the ideal gas law. The non-dimensional Euler-equations in vectorial form and curvilinear coordinates can be written as

$$\frac{\partial \mathbf{Q}}{\partial \tau} + \frac{\partial \mathbf{F}}{\partial \xi} + \frac{\partial \mathbf{G}}{\partial \eta} + \frac{\partial \mathbf{H}}{\partial \zeta} = 0, \tag{5}$$

Using the conservative variables the system of partial differential equations is closed by the ideal gas equation:

$$p = (\kappa - 1)\left[e - \frac{1}{2\rho}\left((\rho u)^2 + (\rho v)^2 + (\rho w)^2\right)\right]. \tag{6}$$

Splitting the unsteady coordinates and flow quantities into a steady reference part and a disturbance part leads to the time-linearization of the Euler-equations in eq. (5). Using a harmonic approach for the disturbance part in terms of this linearization, the coordinates for harmonic motion can be written as

$$\mathbf{x}(\xi,\eta,\zeta,\tau) = \overline{\mathbf{x}}(\xi,\eta,\zeta) + \hat{\mathbf{x}}(\xi,\eta,\zeta) \cdot e^{ik_{red}\tau} \tag{7}$$

In a similar way, the flow quantities can be written as

$$\begin{aligned}\mathbf{Q} &= \overline{\mathbf{Q}} + \hat{\mathbf{Q}} \cdot e^{ik_{red}\tau} \\ \mathbf{F} &= \overline{\mathbf{F}} + \hat{\mathbf{F}} \cdot e^{ik_{red}\tau} \\ \mathbf{G} &= \overline{\mathbf{G}} + \hat{\mathbf{G}} \cdot e^{ik_{red}\tau} \\ \mathbf{H} &= \overline{\mathbf{H}} + \hat{\mathbf{H}} \cdot e^{ik_{red}\tau}\end{aligned} \tag{8}$$

using the metrics with the Jacobi-determinant J in form of

$$J = \overline{J} + \hat{J} \cdot e^{ik\tau}. \tag{9}$$

The disturbance part of the conservative variables in eq. (8) can be split into an unknown part consisting of the disturbance part of the flow quantities and the steady reference part of the metrics (superscript $^{(1)}$). The remaining, known part consists of the steady part of the flow quantities and the disturbance metrics (superscript $^{(2)}$). Assuming that the steady reference parts of the flow satisfies the Euler-equations (eq.(5)), the linearized Euler-equation can be written in the frequency domain, using eq. (7) to eq. (9):

$$\begin{aligned}&\frac{\partial \hat{\mathbf{Q}}^{(1)}}{\partial \tau} + \frac{\partial \hat{\mathbf{F}}^{(1)}}{\partial \xi} + \frac{\partial \hat{\mathbf{G}}^{(1)}}{\partial \eta} + \frac{\partial \hat{\mathbf{H}}^{(1)}}{\partial \zeta} = \\ &\qquad - \left(\hat{\mathbf{Q}}^{(1)} ik_{red} + \hat{\mathbf{Q}}^{(2)} ik_{red} + \frac{\partial \hat{\mathbf{F}}^{(2)}}{\partial \xi} + \frac{\partial \hat{\mathbf{G}}^{(2)}}{\partial \eta} + \frac{\partial \hat{\mathbf{H}}^{(2)}}{\partial \zeta} \right).\end{aligned} \tag{10}$$

The nonlinear Euler equations (eq.(5)) are solved with the numerical solver *AER-Eu*, while the linearized Euler-equations (eq.(10)) are solved with *AER-SDEu*. Both CFD solvers were developed at the Institute of Aerodynamics and Fluid Mechanics at the Technical University of Munich [15]. Thereby, the small disturbance solver *AER-SDEu* uses the steady, nonlinear reference solution from *AER-Eu* and deformed meshes (to obtain the disturbed metrics) in order to compute the disturbed flow quantities.

The numerical process for the solution of the nonlinear and the linearized Euler-equations uses a cell-centered finite-volume method. In the given methods *AER-Eu* and *AER-SDEu*, the control volumes are defined by hexahedral, structured CFD meshes. An Upwind Flux Difference Splitting scheme (see Roe [22]) is used for the discretization of the fluxes. A MUSCL-extrapolation provides a second order spacial accuracy of the method (see Kreiselmaier and Laschka [15]). The appearance of physically not plausible oscillations close to nonlinear phenomena as shocks is eliminated by Total-Variation-Diminishing (TVD) (cf. Blazek [4]). The method employs an implicit temporal integration with a LU-SSOR method (cf. Kreiselmaier and Laschka [15] and Pechloff and Laschka [20]).

Using the results from *AER-Eu* and *AER-SDEu*, the forces acting on a cell center (ξ_m, η_m, ζ_m) of a CFD mesh cell due to harmonic motion of mode i can be written as

$$\mathbf{f}_{SD,i}(Ma_\infty, ik_{red}) = \overline{c}_p \cdot \overline{\mathbf{dS}} + \hat{c}_{p,i} \cdot \overline{\mathbf{dS}} + \overline{c}_p \cdot \hat{\mathbf{dS}}_i. \tag{11}$$

Therefore, the disturbance part of the forces for a CFD mesh cell can be written as

$$\hat{\mathbf{f}}_{SD,i}(Ma_\infty, ik_{red}) = \hat{c}_{p,i} \cdot \overline{\mathbf{dS}} + \overline{c}_p \cdot \hat{\mathbf{dS}}_i. \tag{12}$$

The complex generalized aerodynamic forces (GAFs) for mode j and generalized with mode i can be computed using the disturbance forces from eq. (12) and the modal deformation $\hat{\mathbf{z}}_i$ of mode i by

$$
\begin{aligned}
GAF_{ij}(Ma_\infty, ik_{red}) = & \int_S \overline{c}_p \cdot \hat{\mathbf{z}}_i \cdot \hat{\mathbf{dS}}_j \\
& + i \cdot \left(\int_S Re(\hat{c}_{p,j}) \cdot \hat{\mathbf{z}}_i \cdot \overline{\mathbf{dS}} + \int_S Im(\hat{c}_{p,j}) \cdot \hat{\mathbf{z}}_i \cdot \overline{\mathbf{dS}} \right).
\end{aligned} \tag{13}
$$

3. Development of a Correction Method

The Doublet-Lattice-Method is widely used in the industry to determine the aeroelastic behavior of aircraft configurations. The method is applicable to configurations of various complexity and is thereby robust, provides conservative results and requires only little computational effort. This especially qualifies the DLM for an application in development stages of new aircraft, where their structural configuration and geometrical shape undergo significant changes. Although linearized CFD codes as *AER-SDEu* are capable of providing results of higher accuracy than the DLM and predict the aeroelastic behavior more accurately [25], a lot of effort regarding the mesh generation and computations is required, especially when the configuration is changed significantly. The authors therefore propose a correction method to correct Doublet-Lattice unsteady results with results from a linearized CFD method in this section.

Several other correction methods (see for example Giesing et al. [8] and Jadic, Hartley and Giri [13]) show that a purely diagonal multiplicative correction matrix lacks the ability of changing the results qualitatively and to incorporate multiple modes. Thus, when the distribution of the results from both methods differs qualitatively due to geometric effects or shock phenomena, a purely diagonal correction matrix can not sufficiently improve the results of the less accurate aerodynamic method. Other approaches for correction factor techniques therefore suggest fully populated correction matrices (see Jadic, Hartley and Giri [13]). Using fully populated correction matrices, these methods are capable of changing the results quantitatively and qualitatively.

Since these correction methods do not have any constraints to the structure of the correction matrix, it is possible that the off-diagonal terms become unreasonably high and qualitative distribution of the results may be changed in an undesired or unphysical way. Therefore, the following approach employs a fully populated, diagonal dominant correction matrix. The concept of a diagonal dominant correction matrix assures that qualitative corrections are as small as possible and thus prevents unphysical distributions of the corrected values. Furthermore it is possible to introduce the data of several modes into the correction. Computing this correction matrix, the method uses Doublet Lattice results and small disturbance CFD results in the frequency domain. Thus, the correction matrices are dependent on the reduced frequency k_{red} and the Mach number Ma_∞.

The correction matrix is computed to equal the corrected DLM forces for each box and the linearized CFD results splined on the DLM boxes. The correction matrix is thereby either applied to the downwash of the DLM (downwash correction) or the forces of the DLM (force correction). Both approaches are presented in this section. Results from *AER-SDEu* are chosen as representative results for linearized CFD methods. However, the correction is also applicable using other frequency domain CFD methods.

At first, the authors present a general approach to correct a matrix of results $\mathbf{W}_b$ from a particular aerodynamic method using a matrix of results $\mathbf{W}_a$ obtained by an aerodynamic method of higher order. In both matrices, the aerodynamic data is arranged column-wise. The indices a and b indicate the two aerodynamic methods providing the results. Thereby, b denotes the method to be corrected, while method a provides the higher order aerodynamic data for the correction. In general, $\mathbf{W}_a$ and $\mathbf{W}_b$ are of the dimension $n \times m$ with $n > m$.

3.1 Mathematical Approach

The correction is used to improve the accuracy of the results from the less accurate aerodynamic method using a multiplicative correction matrix $\mathbf{C}$ in form of

$$\mathbf{W}_a = \mathbf{C} \cdot \mathbf{W}_b \tag{14}$$

The matrices are dependent on the reduced frequency k_{red} and the Mach number Ma_∞:

$$\begin{aligned} \mathbf{W}_a &= \mathbf{W}_a(Ma_\infty, k_{red}), \\ \mathbf{W}_b &= \mathbf{W}_b(Ma_\infty, k_{red}) \\ \mathbf{C} &= \mathbf{C}(Ma_\infty, k_{red}). \end{aligned} \tag{15}$$

Although not explicitly shown, the matrices are dependent on further aerodynamic parameters of the steady flight state as the angle of attack α and the sideslip angle β. The correction matrix $\mathbf{C}$ is of dimension $n \times n$.

As described above, the approach is based on diagonal dominant matrices. Thus, the correction matrix can be written as

$$\mathbf{C} = \mathbf{\Lambda} + \mathbf{\Delta} \tag{16}$$

with

$$\mathbf{\Lambda} = \begin{bmatrix} \lambda_1 & & & 0 \\ & \lambda_2 & & \\ & & \ddots & \\ 0 & & & \lambda_n \end{bmatrix}. \tag{17}$$

In eq. (16), $\mathbf{\Lambda}$ denotes the diagonal correction terms and $\mathbf{\Delta}$ describes the off-diagonal terms of the correction. $\mathbf{\Lambda}$ and $\mathbf{\Delta}$ both are of dimension $n \times n$. To introduce a greater flexibility for the diagonal part of the correction, the approach contains n various correction terms λ_i in a diagonal correction matrix $\mathbf{\Lambda}$.

In general, λ_i, $\mathbf{\Lambda}$ and $\mathbf{\Delta}$ are also dependent on the Mach number, the reduced frequency and further aerodynamic parameters of the steady flight condition (as for example α and β). Using eq. (16), the identity of the results of both methods of eq. (14) can be written as

$$\mathbf{\Delta} \cdot \mathbf{W}_b = \mathbf{W}_a - \mathbf{\Lambda} \cdot \mathbf{W}_b \qquad \text{with} \qquad n > m. \tag{18}$$

Eq. (18) describes an under-determined system of equations since $n \cdot m \leq n^2$. Therefore, a least-squares method is used to compute $\mathbf{\Delta}$ depending on $\mathbf{\Lambda}$ in order to obtain $\mathbf{C}$ with the smallest deviation from a perfectly matching correction. Employing a least-squares method in form of a Moore-Penrose Pseudo-Inverse (cf. Moore[17] and Penrose[21]) leads to

$$\mathbf{\Delta} = (\mathbf{W}_a - \mathbf{\Lambda}\mathbf{W}_b) \cdot \left[\left(\mathbf{W}_b^H \mathbf{W}_b \right)^{-1} \right]^H \mathbf{W}_b^H \tag{19}$$

The diagonal part $\mathbf{\Lambda}$ of the correction matrix consisting of $\lambda_1 \ldots \lambda_n$ is computed using

$$\mathbf{a}_i = \begin{Bmatrix} \mathbf{W}_a(i,1) \\ \mathbf{W}_a(i,2) \\ \vdots \\ \mathbf{W}_a(i,m) \end{Bmatrix} \tag{20}$$

and

$$\mathbf{b}_i = \begin{Bmatrix} \mathbf{W}_b(i,1) \\ \mathbf{W}_b(i,2) \\ \vdots \\ \mathbf{W}_b(i,m) \end{Bmatrix}. \tag{21}$$

Since $\mathbf{a}_i = \lambda_i \mathbf{b}_i$, an over-determined least-squares regression problem is solved by using a Gauss-transformation[27], leading to

$$\mathbf{\Lambda}(Ma_\infty, k_{red}) = diag\left(\frac{\mathbf{b}_i^H \mathbf{a}_i}{\mathbf{b}_i^H \mathbf{b}_i}\right) \text{ with } i = 1, 2, \dots, n. \tag{22}$$

Thus, a diagonal dominant, fully populated correction matrix can be obtained by

$$\mathbf{C} = \mathbf{\Lambda} + (\mathbf{W}_a - \mathbf{\Lambda W}_b) \cdot \left[\left((\mathbf{W}_b)^H \mathbf{W}_b\right)^{-1}\right]^H \mathbf{W}_b^H. \tag{23}$$

In sum, the correction matrix $\mathbf{C}$ consists of a diagonal correction obtained from eq. (22) and an off-diagonal correction part obtained from a least squares solution of the resulting residuals from the diagonal correction (see eq. (23)).

3.2 Correction of DLM Results with Small-disturbance CFD Aerodynamics

The general approach and the mathematics for a diagonal dominant correction matrix as presented above are now used to formulate an equation for a correction matrix improving DLM results using modal small-disturbance CFD aerodynamics in frequency domain from *AER-SDEu*. The approach emanates from an equality of forces between the forces acting on the DLM panels modified by the correction matrix and the forces acting on the CFD-mesh surface cells splined onto the DLM boxes (see eq. (24)). Thus, a conservation of forces is guaranteed. The correction matrix $\mathbf{C}_W$ does not correct the forces itself, but the matrix of downwash vectors for multiple modes of the DLM method (similar to the so called *postmultiplicative correction matrices* described by Giesing et al. [8]). An approach to correct the forces itself by using a correction matrix $\mathbf{C}_F$ is described and investigated additionally.

The equality of forces for the downwash correction writes

$$\mathbf{G}^T \mathbf{F}_{SD} = \mathbf{S} \cdot \mathbf{AIC} \cdot \mathbf{C}_W \frac{\mathbf{W}}{U_\infty}, \tag{24}$$

and for the force correction

$$\mathbf{G}^T \mathbf{F}_{SD} = \mathbf{C}_F \cdot \mathbf{S} \cdot \mathbf{AIC} \frac{\mathbf{W}}{U_\infty}, \tag{25}$$

with $\mathbf{C}_W$ indicating the correction matrix for the downwash correction and $\mathbf{C}_F$ the correction matrix for the force correction. In eq. (24) and eq. (25), $\mathbf{S}$ describes the diagonal matrix of surface areas of the DLM boxes, $\mathbf{AIC}$ the matrix of aerodynamic influence coefficients obtained from the DLM and $\mathbf{G}^T$ the splining interpolation matrix used to interpolate the aerodynamic forces from the CFD-mesh surface cells to the DLM boxes. $\mathbf{S}$ and $\mathbf{AIC}$ are of dimension $n \times n$, $\mathbf{W}$ is of the dimension $n \times m$, $\mathbf{F}_{SD}$ is of the dimension $l \times m$ and $\mathbf{G}^T$ is of the dimension $n \times l$. Applied to a correction method between DLM and CFD methods, n describes the number of DLM boxes, m denotes the number of modes selected for the correction and l indicates the number of CFD-mesh surface cells.

In eq. (24) and eq. (25), the matrix $\mathbf{F}_{SD}$ consists of the modal data of multiple modes from the small-disturbance CFD-method in form of

$$\mathbf{F}_{SD} = \left[\mathbf{f}_{SD,1}, \mathbf{f}_{SD,2}, \dots, \mathbf{f}_{SD,m}\right]. \tag{26}$$

Thereby, the correction only uses the parts of the disturbance forces from eq. (12) resulting from the disturbance pressure distribution, namely

$$\mathbf{f}_{SD,i} = \hat{c}_{p,i} \cdot \overline{\mathbf{dS}} \tag{27}$$

for a single CFD mesh cell. Since the DLM does not compute the part of the disturbance forces based on the steady pressure distribution, these parts are not inherently present in the DLM. Nevertheless, they can be added to the DLM through an additive correction term, which is not followed here. Furthermore, $\mathbf{G}^T\mathbf{F}_{SD}$ does only contain the parts of the splined disturbance forces normal to the DLM panels to avoid the introduction of unphysical force distributions.

The matrix $\mathbf{W}$ consists of the downwash vectors for multiple modes of the DLM in form of

$$\mathbf{W}(k_{red}) = \left[\mathbf{w}_1(k_{red}), \mathbf{w}_2(k_{red}), \ldots, \mathbf{w}_m(k_{red})\right]. \tag{28}$$

The matrix $\mathbf{W}$ depends only on the reduced frequency.

Using the balance of forces described above, a conservation of forces normal to the DLM panels is assured. A conservation of the moments around the three axes can not be inherently guaranteed since only the forces normal to the DLM panels are used. However, the losses in accuracy of the moments are expected to be small, especially for M_x, because it is mainly influenced by these normal forces. Despite these effects, a significant improvement of accuracy of the DLM results is expected compared to the uncorrected DLM results.

Assuming that $\mathbf{AIC}$ and $\mathbf{S}$ are invertible in general, one obtains

$$\mathbf{AIC}^{-1}\mathbf{S}^{-1}\mathbf{G}^T\mathbf{F}_{SD} = \mathbf{C}_W \frac{\mathbf{W}}{U_\infty}, \tag{29}$$

for the downwash correction. The equation for the force correction remains as written in eq. (25). The correction matrix for the downwash correction $\mathbf{C}_W$ can thus be obtained by

$$\begin{aligned}\mathbf{C}_W(Ma_\infty, k_{red}) = \mathbf{\Lambda} + \left(\mathbf{AIC}^{-1}\mathbf{S}^{-1}\mathbf{G}^T\mathbf{F}_{SD} - \frac{1}{U_\infty}\mathbf{\Lambda}\mathbf{W}\right) \\ \cdot \frac{1}{U_\infty^3}\left[\left(\mathbf{W}^H\mathbf{W}\right)^{-1}\right]^H \cdot \mathbf{W}^H\end{aligned} \tag{30}$$

and the matrix $\mathbf{C}_F$ for the force correction

$$\begin{aligned}\mathbf{C}_F(Ma_\infty, k_{red}) =& \mathbf{\Lambda} + \left(\mathbf{G}^T\mathbf{F}_{SD} - \frac{1}{U_\infty}\mathbf{\Lambda}\cdot\mathbf{S}\cdot\mathbf{AIC}\cdot\mathbf{W}\right) \\ &\cdot \frac{1}{U_\infty^3}\left[\left(\left[\mathbf{S}\cdot\mathbf{AIC}\cdot\mathbf{W}\right]^H\left[\mathbf{S}\cdot\mathbf{AIC}\cdot\mathbf{W}\right]\right)^{-1}\right]^H \\ &\cdot \left[\mathbf{S}\cdot\mathbf{AIC}\cdot\mathbf{W}\right]^H.\end{aligned} \tag{31}$$

Thus, a correction matrix $\mathbf{C}_W$ or $\mathbf{C}_F$ is computed for each desired value of the reduced frequency k_{red} and Mach number Ma_∞. The entries of the correction matrices are complex values. The real part of the correction matrix introduces a scaling of the real and imaginary DLM data, while the imaginary part results from a phase shift between DLM and CFD data and thus corrects the phase of the DLM data.

Using the approach described above, the correction matrices in general consist of dominant diagonal entries and small off-diagonal entries. However, the detailed structure of the matrices depends on the number and geometric properties of the modes used to compute the correction. Moreover, the structure of the matrices varies with the Mach number and the reduced frequency. Since it is possible to introduce literally any set of modes, the included modes should form a modal base without linearly dependent modes. Furthermore,the combination of modes should at least contain one non-zero downwash entry for each box of the DLM model. Thus, unreasonably high correction factors can be prevented. In an ideal case, the modal data should be chosen to represent the flutter mechanism of the respective configuration for optimal correction results. However, the authors already expect significant improvements through the correction even when only modes similar to the flutter mechanism are used (e.g. plunge and pitch rigid body modes).

Since several analyses showed that results for DLM aerodynamics and small-disturbance CFD aerodynamics differ about $10-15\%$ in the GAF-entries (cf. Vidy et al. [25]), the authors expect diagonal entries of $0 \leq \mathbf{C}_W(i,i) \leq 2$ and $0 \leq \mathbf{C}_F(i,i) \leq 2$ with $i = 1 \ldots n$ in the correction matrices. Large correction factors are expected at the leading edge of the wing and in areas with downwash entries close to zero.

4. Results

The following section presents the application and the respective results of the correction method developed in sec. 3.2 to two configurations, namely the AGARD Wing 445.6 (weak. 3) and the Goland+ Wing.

4.1 AGARD Wing 445.6 (weak. 3)

The AGARD Wing 445.6 is a three-dimensional wing structure (half model) providing wing thickness effects for the correction on its symmetric airfoil. Furthermore, the flutter characteristics of the configuration show a significant drop in flutter speed in the transonic flow regime (transonic dip) [14]. Since experimental flutter data is available for the configuration [14] and the linearized Euler-Code *AER-SDEu* has been applied to the configuration in the past (cf. Fleischer et al. [7], Vidy et al. [25] and Fleischer [5]), the AGARD Wing 445.6 serves as a test case for the correction method.

The CFD mesh for the AGARD Wing was generated with Ansys ICEM CFD as a two-block C-H topology with a total of 532480 mesh cells, of which 6768 cells represent the surface of the configuration. The off-body distance of the first cell row is $h_{OBD} = 10^{-3} \cdot c_r$. The surface mesh with the symmetry plane is shown in fig. 1 a). The DLM model consists of 100 boxes with a distribution of 10 boxes in spanwise direction and 10 boxes in chordwise direction. The distributions are equally spaced in both directions. The DLM model is shown in fig. 1 b). The boxes of the DLM model are numbered from 1 to 100 following the numbering approach given in [18] . Details on the steady and unsteady pressure distributions for various Mach numbers and reduced frequencies, the flutter and gust results obtained with both methods are given by Fleischer and Breitsamter [6] and Vidy et al. [25].

The deformed CFD meshes for the linearized CFD solver *AER-SDEu* are generated with MatLab from the undeformed CFD mesh and the structural eigenmodes from a FEM-computation with MSC-NASTRAN. Thereby, the deformations of the structural model are transferred to the CFD surface mesh through a spline interpolation [26], and to the volume mesh through a transfinite interpolation (TFI)[16] and a spring analogy [12]. The FEM model complies with the structural characteristics of the wing defined by Yates [14].

At first, it is validated that the interpolation of the disturbance forces obtained with the CFD method does not produce any unphysical force distributions on the DLM boxes. Afterwards, the distribution of the disturbance forces from the DLM and *AER-SDEu* are compared to obtain a first assessment of the structure of the correction matrix.

As an example, fig. 2 compares the real part of the disturbance forces for the 2nd and 3rd elastic mode obtained with the DLM to the results obtained with *AER-SDEu* splined onto the DLM model. Despite the high Mach number,

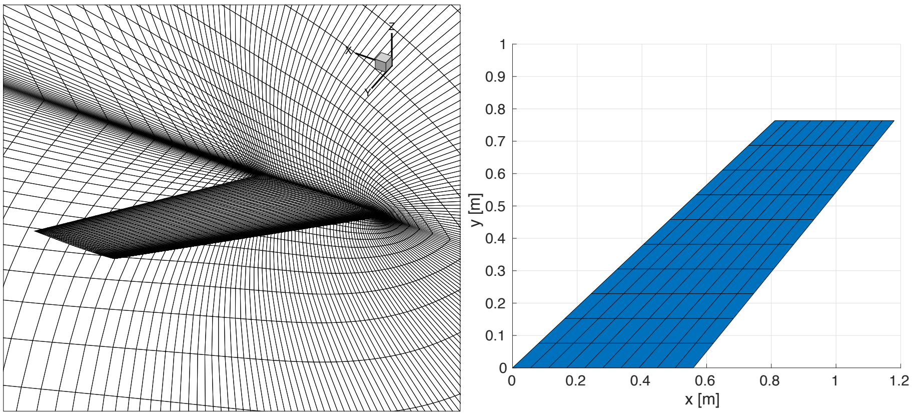

(a) CFD surface mesh and symmetry plane (b) DLM model

Figure 1: CFD mesh and DLM model of the AGARD Wing 445.6 (weak. 3)

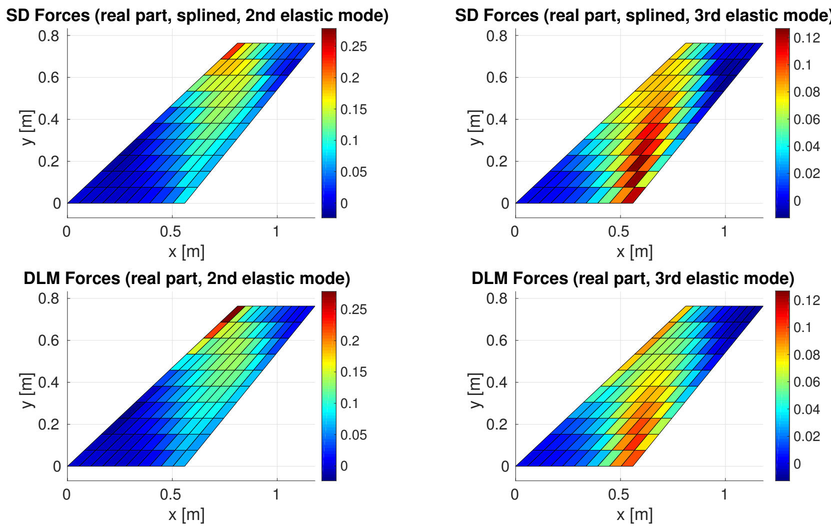

Figure 2: Real part of the disturbance forces (eq. (27)) from *AER-SDEu* and the DLM for the 2nd and 3rd elastic mode of the AGARD Wing; $Ma_\infty = 0.954$, $k_{red} = 0.5$

the force distributions do not show any discontinuities. Furthermore, the force distributions of both methods match qualitatively, which is expected to lead to small off-diagonal terms in the correction matrix. Since the DLM assumes large leading edge suction effects due to the neglect of thickness effects, the DLM predicts forces of higher magnitude than *AER-SDEu* at the leading edge of the configuration (see fig. 2). However, *AER-SDEu* predicts forces of higher magnitude towards the trailing edge and the wing tip of the configuration (see fig. 2). Since each diagonal entry directly belongs to a respective box of the DLM model, these effects lead to the expectation of diagonal entries below one ($\mathbf{C}_W < 1$) for leading edge boxes and diagonal entries above one ($\mathbf{C}_W > 1$) for trailing edge boxes.

Correction matrices were computed using the approach of sec. 3.2 for the Mach numbers $Ma_\infty = 0.499, 0.678, 0.901, 0.954$, the reduced frequencies $k_{red} = 0.0, 0.01, 0.1, 0.3, 0.5, 1.0, 3.7$ and several combinations of modes. The latter are listed in tab. 1. Fig. 3 shows the correction matrices obtained for Case 3 of tab. 1 for different Mach numbers and $k_{red} = 0.5$ in their real and imaginary part. The matrices show a diagonal dominant structure for all Mach numbers with small off-diagonal terms, even though several modes are included. The behavior of the diagonal entries regarding the leading edge and trailing edge force distribution of both methods is as expected. The diagonal entries corresponding to the first row of DLM boxes at the symmetry planes show changes of sign with large amplitude. These characteristics result from the fact that the elastic modes show downwash entries close to zero for these boxes, since

Table 1: Mode combinations applied for the correction method on the AGARD Wing 445.6 (weak. 3)

Case	Mode Combination
Case 1	pitch mode
Case 2	1st bending, 1st torsional mode
Case 3	pitch mode, 1st bending, 1st torsional mode
Case 4	pitch mode, first five elastic modes

the model is clamped to the symmetry plane and shows no modal deformation there for the elastic modes.

Fig. 4 shows a comparison of the diagonal entries of the downwash correction matrices for all cases of tab. 1. Again, each diagonal entry directly belongs to a respective box of the DLM model. Case 1 predicts a smoother distribution of the correction factors for the first boxes than the other cases, since it does not show downwash entries close to zero for these boxes. For the boxes representing the center and outer wing, the diagonals match for all cases of tab. 1. It can be noticed that the imaginary entries for Case 1 show greater peaks for boxes assigned to the leading edge and thus introduce a greater phase shift there.

Fig. 5 presents the GAF entries for the first three elastic modes of the AGARD Wing obtained with DLM results, *AER-SDEu* results and downwash corrected DLM results for Case 3. Deviations can be noticed between the DLM results and the *AER-SDEu* results. The correction has the effect of enhancing the accuracy of the DLM GAFs towards the accuracy of the *AER-SDEu* GAFs. While the effect is not as strong for other modes, the enhancement can especially be observed for GAF entries of modes which are used as training modes for the correction (fig. 5).

The flutter mechanism of the AGARD Wing is basically a bending-torsion flutter with the coalescence of the first bending and the first torsional mode. Flutter frequencies obtained with DLM and *AER-SDEu* are plotted in form of the Flutter Frequency Ratio (FFR) [14] in fig. 6. The flutter mechanism can be predicted correctly with results from the DLM as well as from *AER-SDEu*.

Using the corrected generalized aerodynamic forces (GAFs) for all cases with the force and downwash correction respectively, the flutter characteristics of the configuration are determined with a p-k-flutter-method. The flutter results are computed for flight conditions of $Ma_\infty = 0.499$, 0.678, 0.901, 0.954 and the corresponding air densities given in [14]. The results are presented in comparison to DLM and *AER-SDEu* in fig. 6 for the downwash correction and in fig. 7 for the force correction. It can be noticed that the Flutter Speed Indices (FSI) [14] differ around 10% between the DLM and *AER-SDEu*. The downwash correction as well as the force correction close this gap between both methods and enhance the quality of the DLM results towards the results of *AER-SDEu*. Thereby, the corrected results match the results of *AER-SDEu* with high accuracy in their numerical values and their distribution. The transonic dip is captured by the downwash and the force correction for all cases as shown in fig. 6 a) and 7 a).

The downwash correction matches the SD results for all cases with high accuracy. The force correction provides results of comparable accuracy for the cases, which represent the flutter mechanism correctly (Cases 2-4). Although Case 1 correctly captures the distribution of the SD results regarding the transonic dip, it shows the largest deviations to the SD results numerically. These observations also hold true for the Flutter Frequency Ratio (FFR) [14] (fig. 6 b) and 7 b)). Both, the downwash and the force correction correctly capture the flutter mechanism for the various flight conditions.

Thus, the downwash correction predicts the flutter behavior of the configuration with high accuracy, even if only rigid body aerodynamic data in the frequency domain and no information on the aerodynamics of elastic deformations is available. The force correction does only enhance the quality of the results, when the selected modal data represents the flutter mechanism correctly. Therefore, the downwash correction is better suited for the development

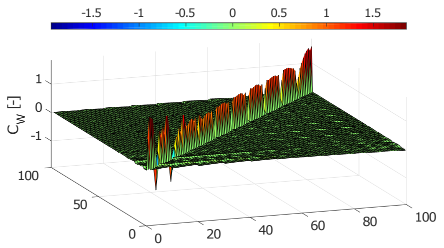

(a) $Ma_\infty = 0.499$, $k_{red} = 0.5$, real part

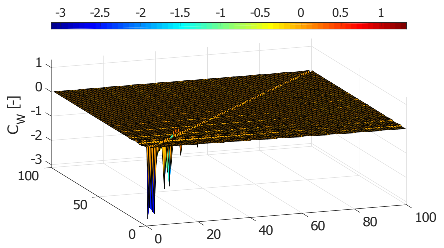

(b) $Ma_\infty = 0.499$, $k_{red} = 0.5$, imaginary part

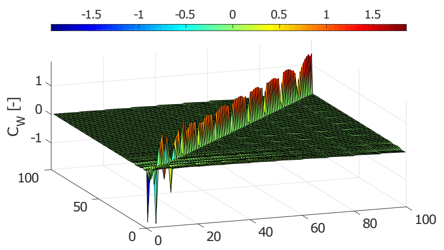

(c) $Ma_\infty = 0.678$, $k_{red} = 0.5$, real part

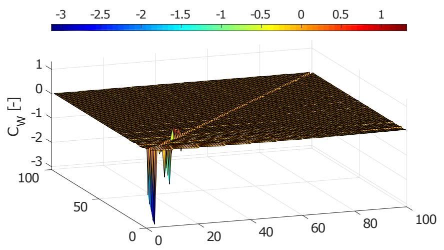

(d) $Ma_\infty = 0.678$, $k_{red} = 0.5$, imaginary part

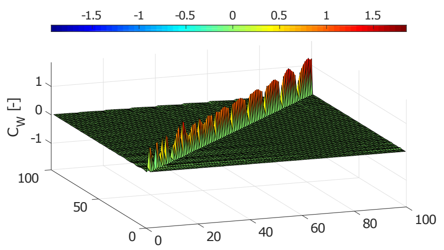

(e) $Ma_\infty = 0.901$, $k_{red} = 0.5$, real part

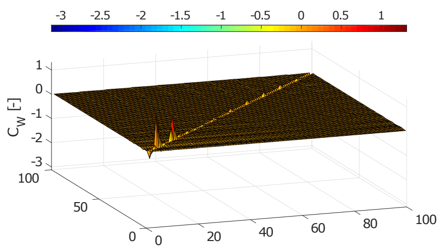

(f) $Ma_\infty = 0.901$, $k_{red} = 0.5$, imaginary part

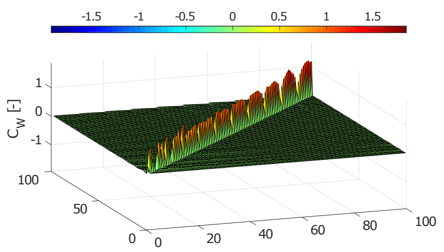

(g) $Ma_\infty = 0.954$, $k_{red} = 0.5$, real part

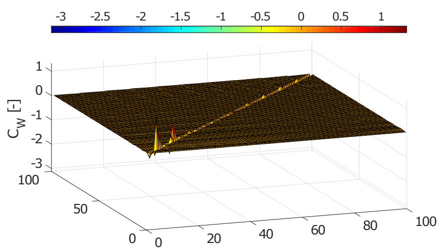

(h) $Ma_\infty = 0.954$, $k_{red} = 0.5$, imaginary part

Figure 3: Real and imaginary parts of the downwash correction matrix for Case 3 for $k_{red} = 0.5$ and different Mach numbers for the AGARD Wing

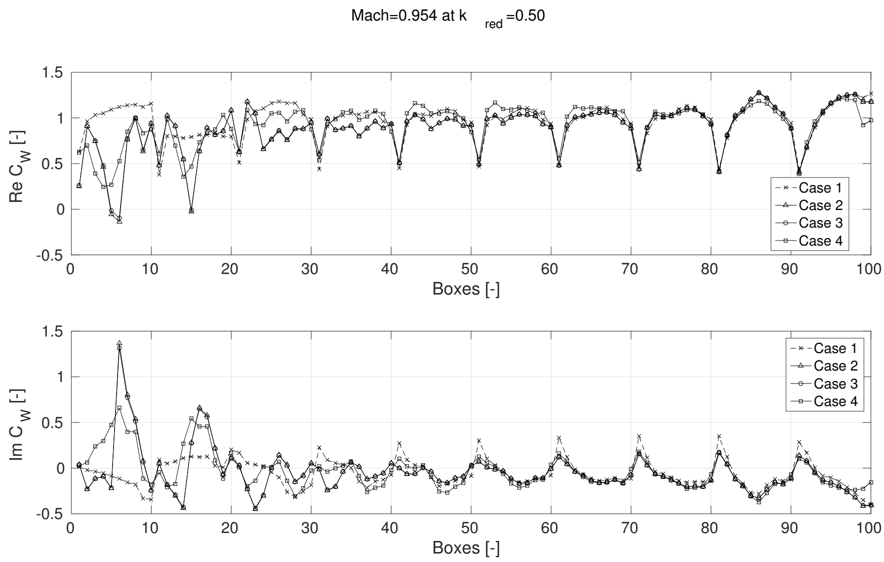

Figure 4: Diagonal entries of the downwash correction matrix for Cases 1-4 for the AGARD Wing for $Ma_\infty = 0.954$, $k_{red} = 0.5$

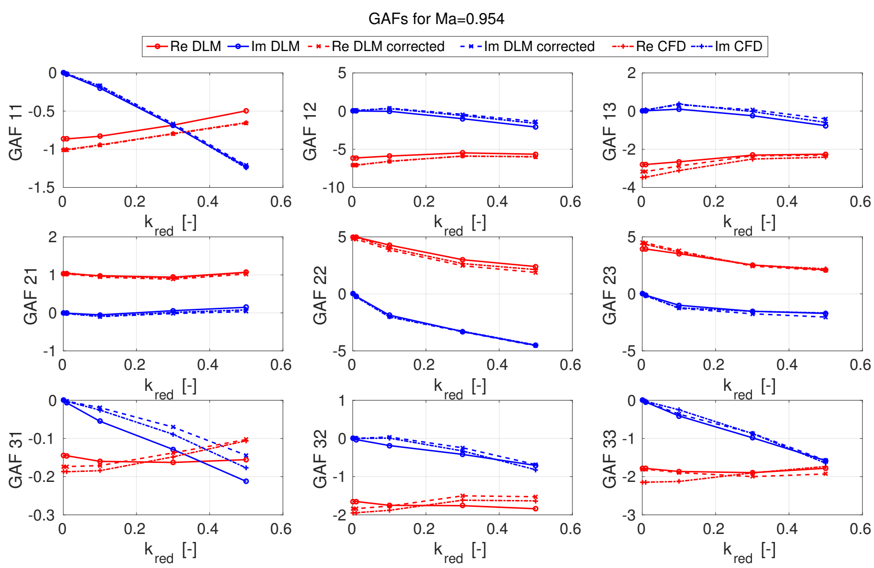

Figure 5: GAFs for the first three modes obtained by DLM, linearized CFD and downwash corrected DLM (Case 3, $\mathbf{C}_W$), $Ma_\infty = 0.954$

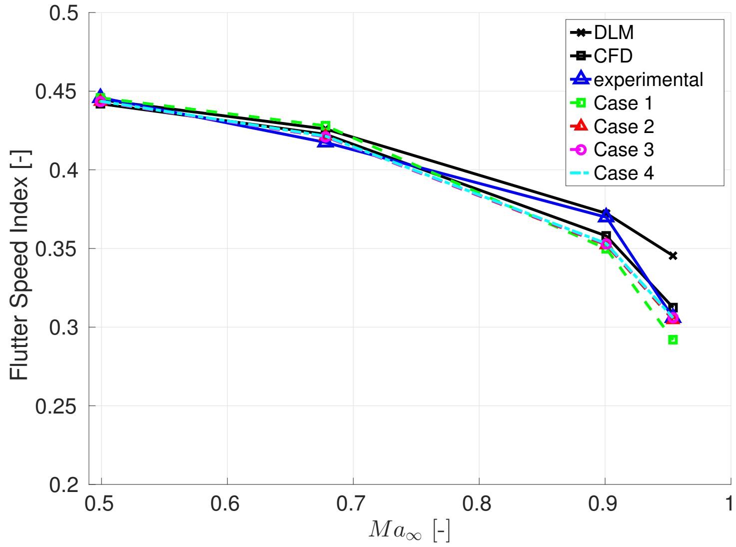

(a) Flutter Speed Index

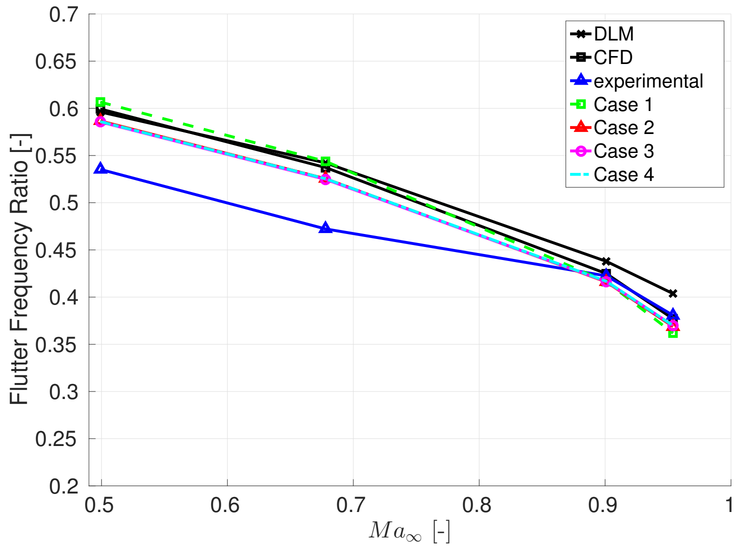

(b) Flutter Frequency Ratio

Figure 6: Flutter Speed Index and Flutter Frequency Ratio using the GAFs of DLM, *AER-SDEu* and the downwash corrected DLM results for Cases 1-4 for the AGARD Wing

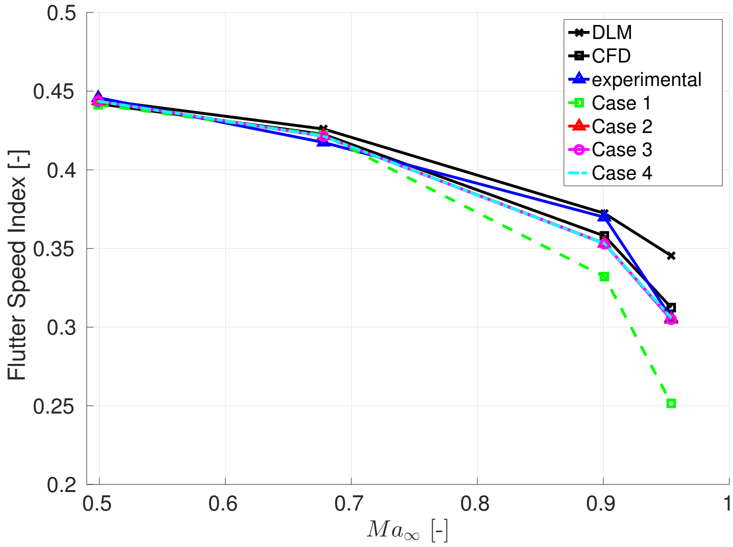

(a) Flutter Speed Index

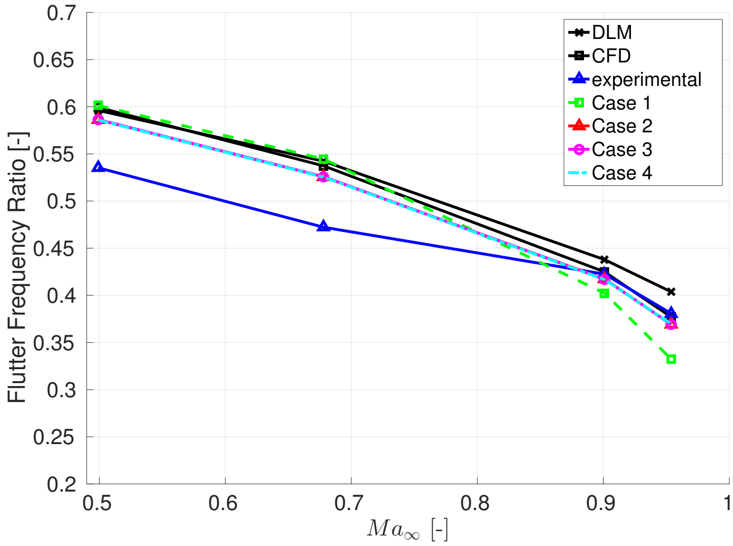

(b) Flutter Frequency Ratio

Figure 7: Flutter Speed Index and Flutter Frequency Ratio using the GAFs of DLM, *AER-SDEu* and the force corrected DLM results for Cases 1-4 for the AGARD Wing

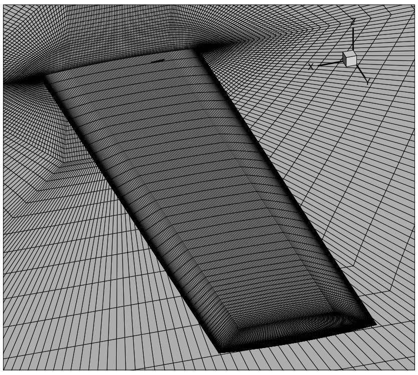

(a) Surface mesh with symmetry plane

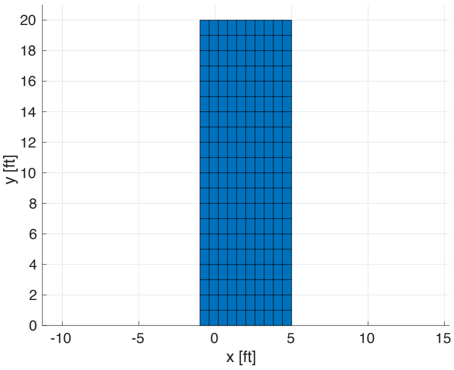

(b) DLM model

Figure 8: CFD mesh of the Goland Wing as surface mesh with symmetry plane and DLM model of the Goland Wing

process of an aircraft, since it significantly enhances the quality of the flutter results even without knowledge of the exact structural behavior of the configuration.

4.2 Goland+ Wing

The Goland Wing provides a configuration with sharp leading and trailing edge on its symmetric, parabolic airfoil in a low transonic flow regime (see Goland [9]). A lot of experience has already been gained with the application of numerical methods to the Goland Wing configuration (see Beran et al. [2] and Snyder et al. [23]). To be consistent with literature results, the data herein is given in the units of the respective literature on the Goland Wing.

The CFD mesh for the Goland Wing was adapted from Snyder et al. [23]. Fig. 8 a) shows the surface mesh of the configuration with the cells on the symmetry plane, while fig. 8 b) shows the DLM model of the configuration. The DLM model consists of 200 boxes with a distribution of 20 boxes in spanwise direction and 10 boxes in chordwise direction. The distributions are equally spaced in both directions. The DLM model is shown in fig. 8 b). The boxes are numbered from 1 to 200, again following the numbering approach given in [18].

The deformed CFD meshes for the modal deformations of the configuration are generated using the undeformed CFD mesh and the structural data from FEM-computations with *MSC-NASTRAN*. The structural model is correctly representing the Goland+ configuration and is adapted from Snyder et al. [23]. As for the AGARD Wing, the modal deformations of the Goland+ Wing are transferred to the CFD surface mesh using a Spline Interpolation (see ZAERO [26]). Afterwards, the deformation of the CFD volume mesh of the farfield is computed using TFI and spring analogy. The deformed meshes are generated for rigid body pitch and plunge deformations, and for the first four elastic modes of the configuration. These modes sufficiently represent the structural behavior of the configuration for aeroelastic analyses and are suitable for the correction.

Again, it is validated that the interpolation of the disturbance forces from the CFD method to the DLM boxes does not result in any unphysical force distributions. In an assessment of the force distributions for both methods as it was performed for the AGARD Wing, similar conclusions can be drawn. As for the AGARD Wing, the distributions match qualitatively with high accuracy and the CFD method predicts forces of higher magnitude at the trailing edge and of lower magnitude at the leading edge than the DLM. Resulting from the sharp leading edge, the deviations between both methods at the leading edge boxes are smaller than observed for the AGARD Wing. As described above, these effects lead to the expectation of diagonal entries below one ($\mathbf{C}_W < 1$) for to the leading edge boxes and diagonal entries above one ($\mathbf{C}_W > 1$) for to the trailing edge boxes.

Table 2: Mode combinations applied for the correction method on the Goland Wing

Case	Mode Combination
Case 1	plunge and pitch mode; with 30% pitch
Case 2	1st bending, 1st torsional mode
Case 3	plunge mode, 1st bending, 1st torsional mode; with 30% pitch
Case 4	plunge mode, all elastic modes; with 30% pitch

Correction matrices were computed using the approach of sec. 3.2 for the Mach numbers $Ma_\infty = 0.5, 0.6, 0.7, 0.8$, the reduced frequencies $k_{red} = 0.0, 0.005, 0.01, 0.02, 0.05, 0.1, 0.2, 0.5, 1.0$ and combinations of modes. The modal combinations are given in tab. 2. For the Cases 1, 3 and 4, a 30%-portion of rigid body pitch is added to every mode other than the pitch mode. Thus, it is ensured that every panel of every mode has a non-zero downwash entry. Therefore, unreasonably high correction factors with changes of sign due to downwash entries close to zero are prevented as observed for the AGARD wing. Effects due to the clamping of the models at the symmetry plane can thus be diminished. Since it is combined with a pitching motion, one can now also use an in-plane mode for the correction. Case 2, namely the introduction of the first two elastic modes, does not involve an addition of a pitching motion to the elastic modes. Thus it is expected that the diagonals for the first boxes are of large magnitude and contain changes of sign for Case 2. Fig. 9 shows the correction matrices obtained for Case 3 of tab. 2 for different Mach numbers and $k_{red} = 0.5$ in their real and imaginary part. As expected, the matrices are of diagonal dominant character for all Mach numbers with small off-diagonal terms, even though several modes are induced. The behavior of the diagonal entries regarding the leading edge and trailing edge force distribution of both methods is as expected.

Fig. 10 compares the diagonal entries of the downwash correction matrices for all cases of tab. 2 involving rigid body modes. Case 2 is not shown because of its unreasonably high correction factors for the first boxes. Despite some trailing edge peaks for Case 4, the diagonals of the presented cases match with high accuracy and show the expected behavior. Although not presented here, the matrices obtained with the force correction show similar behavior to the downwash correction with a smaller drop in at the leading edge.

The flutter mechanism of the Goland+ Wing is a bending-torsion flutter with a coalescence of the first bending and first torsional mode. Flutter frequencies obtained with DLM and *AER-SDEu* are plotted in fig. 11. The flutter mechanism is predicted correctly with results from the DLM and *AER-SDEu*.

Using the corrected GAFs and a p-k-method, corrected flutter results can be computed. Fig. 11 and fig. 12 show the flutter speed and flutter frequency for the downwash and the force correction for varying Mach number and an air density of $\rho = 0.00023771 slugs/ft^3$. It can be observed that the results differ in a very small range between the DLM and *AER-SDEu*. Both methods show a similar behavior in their distributions and their numerical values, as well in flutter frequency as in flutter speed. Despite the small deviations between the DLM and *AER-SDEu*, the correction method still enhances the quality of the DLM results towards the quality of the CFD results. Again, it is observed that the introduction of pure rigid body modal data leads to an enhancement of similar magnitude than the introduction of a full set of rigid body and elastic modes. In the case of the Goland Wing, this holds true for the downwash and the force correction.

Both correction approaches predict smaller flutter frequencies than the original aerodynamic methods for all cases. Nevertheless, the downwash and the force correction correctly capture the flutter mechanism for the various flight conditions.

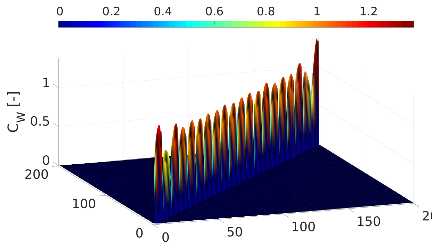

(a) $Ma_\infty = 0.5$, $k_{red} = 0.5$, real part

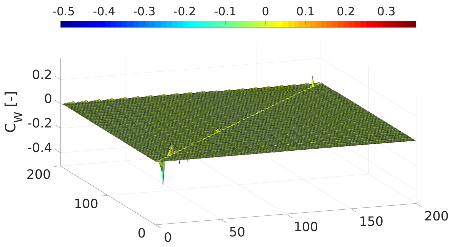

(b) $Ma_\infty = 0.5$, $k_{red} = 0.5$, imaginary part

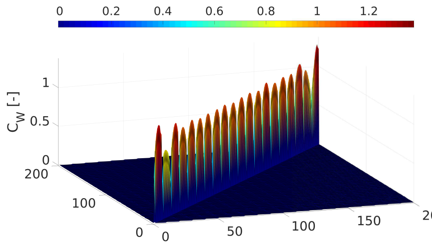

(c) $Ma_\infty = 0.6$, $k_{red} = 0.5$, real part

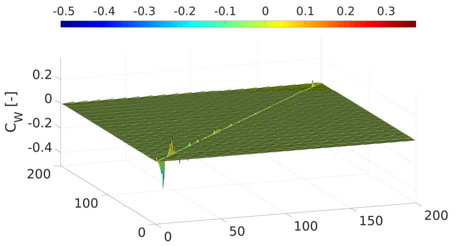

(d) $Ma_\infty = 0.6$, $k_{red} = 0.5$, imaginary part

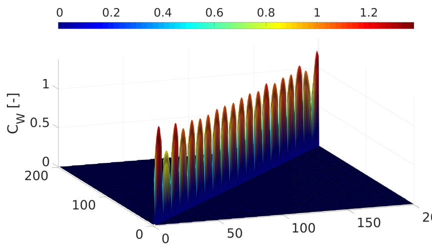

(e) $Ma_\infty = 0.7$, $k_{red} = 0.5$, real part

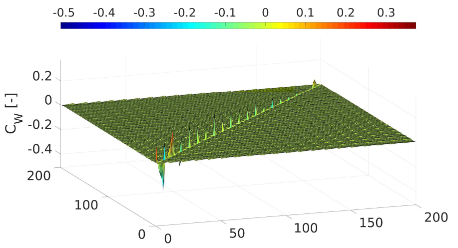

(f) $Ma_\infty = 0.7$, $k_{red} = 0.5$, imaginary part

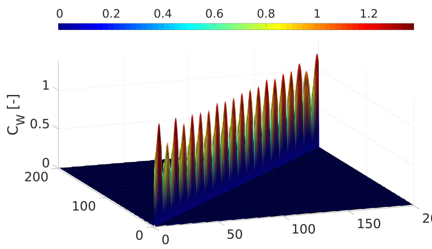

(g) $Ma_\infty = 0.8$, $k_{red} = 0.5$, real part

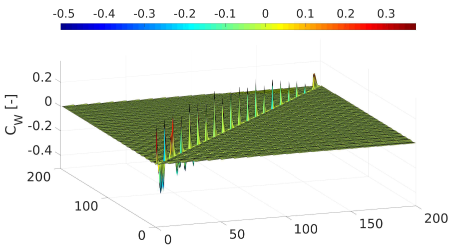

(h) $Ma_\infty = 0.8$, $k_{red} = 0.5$, imaginary part

Figure 9: Real and imaginary parts of the downwash correction matrix for the Goland Wing for Case 3 for $k_{red} = 0.5$ and different Mach numbers

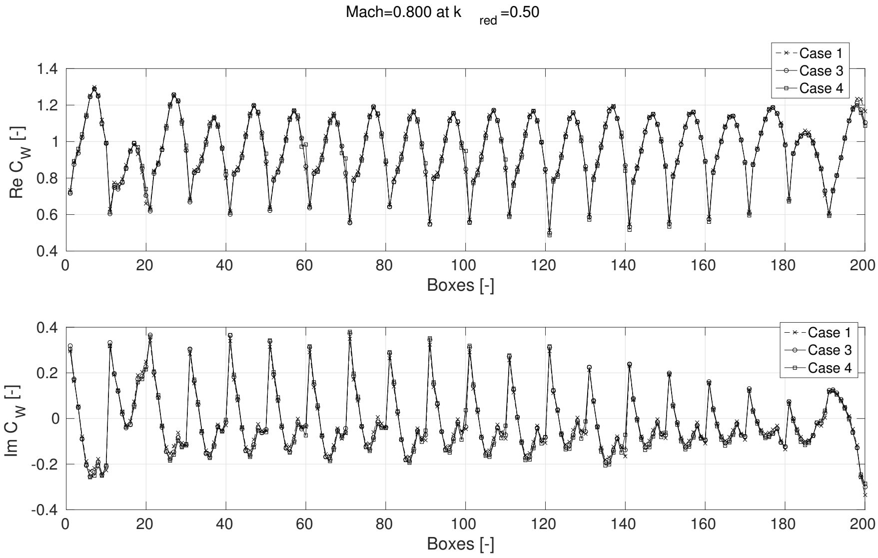

Figure 10: Diagonal entries of the down-wash correction matrix for Cases 1-4 for the Goland+ Wing for $Ma_\infty = 0.8$, $k_{red} = 0.5$

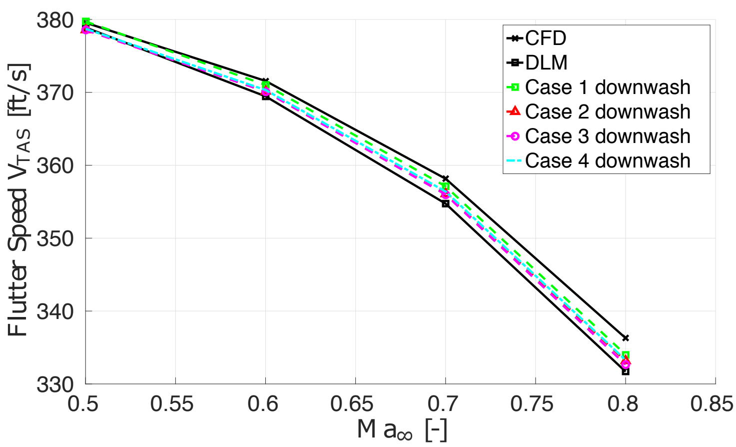

(a) Flutter Speed

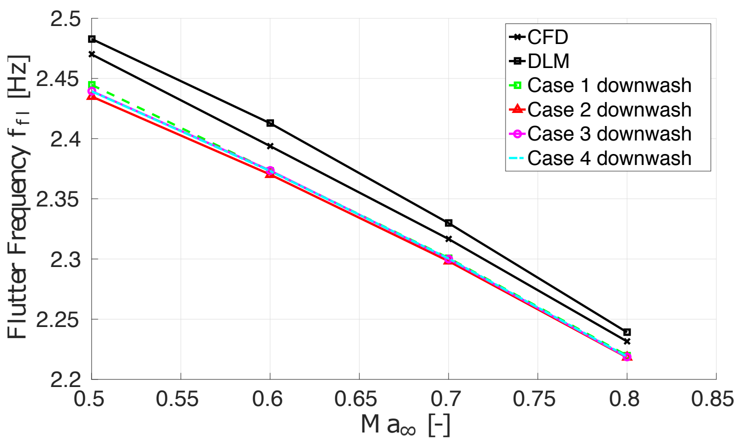

(b) Flutter Frequency

Figure 11: Flutter speed and flutter frequency of the Goland Wing using the GAFs of DLM, *AER-SDEu* and the downwash corrected DLM results for Cases 1-4 at $\rho = 0.00023771 slugs/ft^3 (= 0.1225 kg/ft^3)$

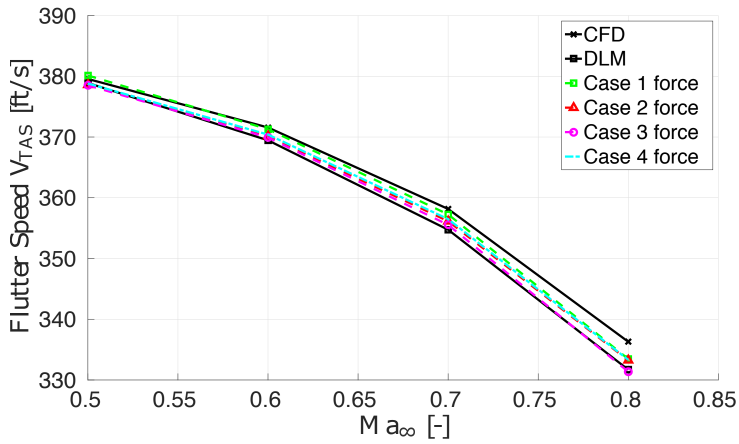

(a) Flutter Speed

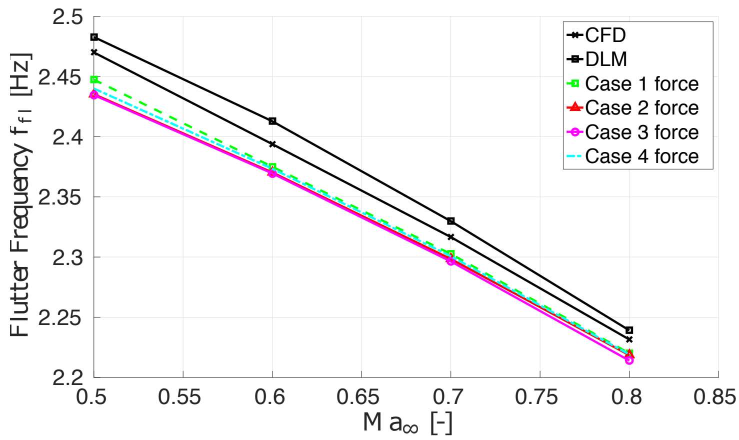

(b) Flutter Frequency

Figure 12: Flutter speed and flutter frequency of the Goland Wing using the GAFs of DLM, *AER-SDEu* and the force corrected DLM results for Cases 1-4 at $\rho = 0.00023771 slugs/ft^3$ ($= 0.1225 kg/ft^3$)

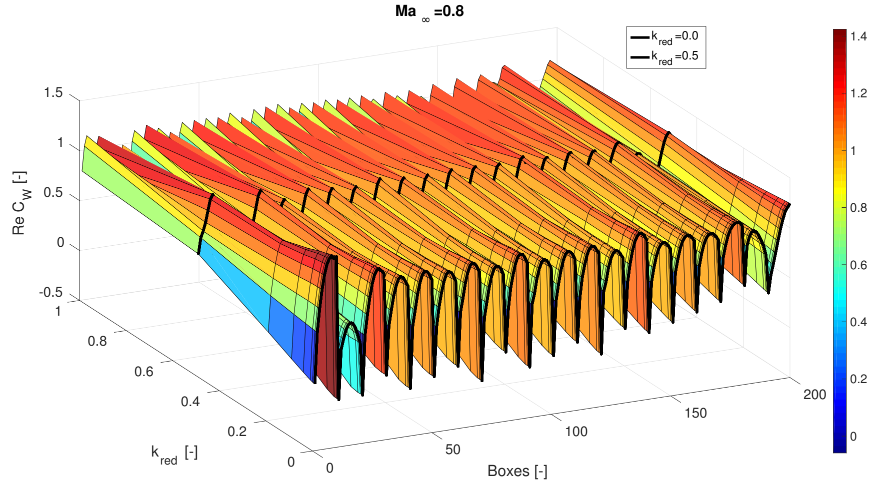

Figure 13: Distribution of the real diagonal entries of $\mathbf{C}_W$ for Case 3 for the Goland Wing over the reduced frequency for $Ma_\infty = 0.954$

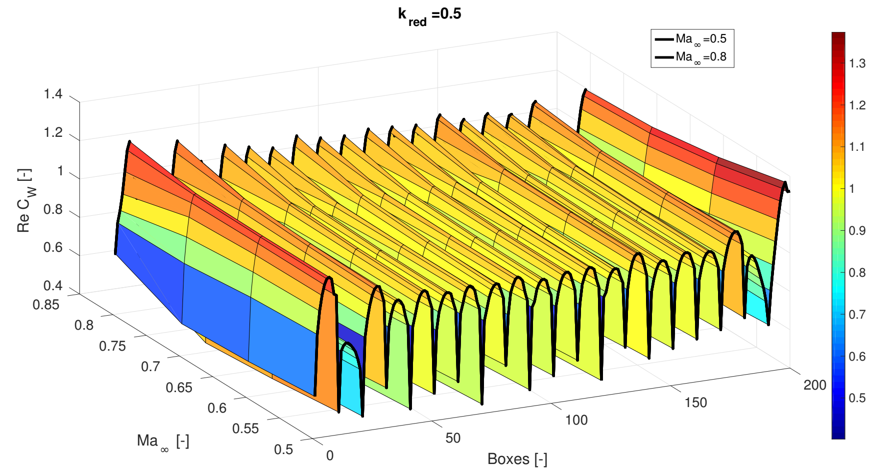

Figure 14: Distribution of the real diagonal entries of $\mathbf{C}_W$ for Case 3 for the Goland Wing over the Mach-number for $k_{red} = 0.5$

4.3 Interpolation of the Correction Matrices

The presented correction method promises to reduce the computational efforts for an aeroelastic analysis compared to purely CFD-based methods during the development phase of aircraft configurations. Further reduction of these computational costs can be achieved by means of interpolating the correction matrices over the reduced frequency and the Mach number. For the Goland Wing in downwash correction Case 3, fig. 13 and 14 present the distribution of the correction diagonals in their real part over the reduced frequency and the Mach number, respectively. The resulting distributions of the correction diagonals over the respective flight parameter are smooth and promise an appropriate interpolation of the correction matrices. Although not presented in this paper, the same effect is observed for the imaginary part of the correction diagonals. Further studies with different interpolation methods have to be conducted.

5. Conclusions

A correction method to enhance the quality of DLM results by introducing small-disturbance CFD aerodynamics was developed and successfully applied to the AGARD Wing 445.6 (weak. 3) and the Goland+ Wing. The method employs fully populated, diagonal dominant correction matrices to minimize the change in the qualitative distribution of the DLM results and enables the correction to use several modal data at the same time. The authors showed in a first step that the developed method is robust and enhances the DLM results even for the sole injection of rigid body modes. This results prove the applicability of the method during the development process of aircraft configurations. Further studies have to be conducted using configurations of higher complexity, an additive correction part and interpolation of the correction matrices.

Acknowledgements

The authors would like to express their gratitude to Dr. Daniele Parisse and Dr. Dietmar Fleischer from Airbus Defence and Space for their contribution to the mathematics and the results of the present paper.

References

[1] E. Albano and W. P. Rodden. *A Doublet-Lattice Method for Calculating Lift Distributions on Oscillating Surfaces in Subsonic Flows.* AIAA Journal, Vol. 7, Nr. 2, S. 279–285, 1969.

[2] P. S. Beran, N. S. Khot, F. E. Eastep, R. D. Snyder and J. V. Zweber. *Numerical Analysis of Store-Induced Limit-Cycle Oscillation.* AIAA Journal of Aircraft, Vol. 41, Nr. 6, S. 1315–1326, 2004.

[3] M. Blair. *A Compilation of the Mathematics Leading to the Doublet-Lattice-Method.* Wright Laboratory, Wright-Patterson Air Force Base, Ohio, USA, 1991. WL-TR-92-3028.

[4] J. Blazek. *Computational Fluid Dynamics - Principles and Applications.* Elsevier Science Ltd., Kidlington, Oxford, UK, 2001.

[5] D. Fleischer. *Verfahren Reduzierter Ordnung Zur Ermittlung Instationärer Luftkräfte.* PhD Thesis Institute for Aerodynamics, Technical University of Munich, 2014.

[6] D. Fleischer and C. Breitsamter. *Efficient Computation of Unsteady Arodynamic Loads Using Computational-Fluid-Dynamics Linearized Methods.* Journal of Aircraft, Vol. 16, Nr. 2, S. 117–124, 2013.

[7] D. Fleischer, C. Vidy, M. Iatrou, C. Breitsamter and C. Weishäupl. *Linear Flutter Prediction for Low Aspect Ratio Wings Using a Small Disturbance Euler Method.* IFASD International Forum on Aeroelasticity and Structural Dynamics, IFASD-2009-055, 2009.

[8] J. P. Giesing, T. P. Kalman and W. P. Rodden. *Correction Factor Techniques For Improving Aerodynamic Prediction Methods.* NASA, 1976. NASA CR-144967.

[9] M. Goland. *The Flutter of a Uniform Cantilever Wing.* Journal of Applied Mechanics, Vol. 12, Nr. 4, S. A–197 – A–208, 1945.

[10] K. A. Hoffmann and S. T. Chiang. *Computational Fluid Dynamics for Engineers - Volume I.* Engineering Education System, Wichita, KS 67208-1078, USA, 1995.

[11] K. A. Hoffmann and S. T. Chiang. *Computational Fluid Dynamics for Engineers - Volume II.* Engineering Education System, Wichita, KS 67208-1078, USA, 2000.

[12] B. K. Soni J. F. Thompson and N. P. Weatherill. *Handbook of Grid Generation.* CRC Press LLC, 2000 N.W. Corporate Blvd., Boca Raton, Florida 33431, 1999.

[13] I. Jadic, D. Hartley and J. Giri. *An Enhanced Correction Factor Technique for Aerodynamic Influence Coefficient Methods.* MSC's Proceedings of the 1999 Aerospace User's Conference, 1999.

[14] E. C. Yates Jr. *AGARD Standard Aeroelastic Configurations for Dynamic Response. Candidate Configuration I.-Wing 445.6.* NASA Technical Memorandum, 1987. NASA TM-100492.

[15] E. Kreiselmaier and B. Laschka. *Small Disturbance Euler Equations: Efficient and Accurate Tool for Unsteady Load Prediction.* AIAA Journal of Aircraft, Vol. 37, Nr. 5, S. 770–778, 2000.

[16] V. D. Liseikin. *Grid Generation Methods.* Springer, Dodrecht Heidelberg London New York; 2. Auflage, 2010.

[17] E. H. Moore. *On the Reciprocal of the General Algebraic Matrix.* Bulletin of the American Mathematical Society, Vol. 26, , 1920.

[18] MSC.Software GmbH, Am Moosfeld 13, 81829 München. *MSC Nastran Aeroelastic Analysis User's Guide*, 2004.

[19] R. Palacios, H. Climent, A. Karlsson and B. Winzell. *Assessment of Strategies for Correcting Linear Unsteady Aerodynamics Using CFD or Test Results.* IFASD International Forum on Aeroelasticity and Structural Dynamics, IFASD2001-074, 2001.

[20] A. Pechloff and B. Laschka. *Small Disturbance Navier-Stokes Method: Efficient Tool for Predicting Unsteady Air Loads.* Journal of Aircraft, Vol. 43, Nr. 1, S. 17–29, 2006.

[21] R. Penrose. *A General Inverse for Matrices.* Proceedings of Cambridge Philosophical Society, Vol. 51, , 1955.

[22] P. L. Roe. *Approximate Riemann Solvers, Parameter Vectors and Difference Schemes.* Journal of Computational Physics, Vol. 43, Nr. 2, S. 357–372, 1981.

[23] R. D. Snyder, J. N. Scott, N. S. Khot, P. S. Beran and J. V. Zweber. *Predictions of Store Induced Limit-Cycle Oscillations Using Euler and Navier-Stokes Fluid Dynamics.* 44th AIAA/ASME/ASCE/AHS/ASC Structures, Structural Dynamics, and Materials Conference and Exhibit, AIAA-2003-1727, 2003.

[24] R. Thormann and M. Widhalm. *Linear-Frequency-Domain Predictions of Dynamic-Response Data for Viscous Transonic Flows.* AIAA Journal, Vol. 51, Nr. 11, S. 2540–2557, 2013.

[25] C. Vidy, L. Katzenmeier, M. Winter and C. Breitsamter. *Verification of the Use of Small-Disturbance CFD Aerodynamics in Flutter and Gust Analyses for Simple to Highly Complex Configurations.* IFASD International Forum on Aeroelasticity and Structural Dynamics, IFASD-2015-055, 2015.

[26] ZONA Technology, Inc., 9489 E. Ironwood Square Drive, Scottsdale, AZ 85258-4578. *ZAERO Version 8.2 Theoretical Manual*, 18th 03-08 edition, March 2008.

[27] R. Zurmühl and S. Falk. *Matrizen und ihre Anwendungen 1.* Springer-Verlag Berlin Heidelberg, 1997.